Highly Sensitive Implementation of Logic Gates with a Nonlinear Nanomechanical Resonator

Yukihiro Tadokoro[*] and Hiroya Tanaka

Toyota Central R&D Laboratories, Inc., Aichi, Nagakute, 480-1192, Japan

We introduce a theoretical concept of logic gates for sequenced data that contain a large number of data bits to be computed using a nonlinear nanomechanical resonator. Resonantly driven nanomechanical modes display the bistability of forced vibrations. Near the cusp point on the bifurcation curve, even a small change in driving force can lead to switching between the vibrational states with significantly different amplitudes. This enables a highly sensitive implementation of logic gates, including AND, OR, and XOR gates. The underlying principles are simple and generic, suggesting that our method is applicable not only to nanomechanical systems but also to a wide variety of bistable physical, chemical, and biological systems.

I. INTRODUCTION

Nanomechanical systems are attracting attention in various fields owing to their desirable features, including low power consumption and high sensitivity [1,2]. Their fundamental behavior has been discussed mainly in physics; such systems are a good test bed for exploring a number of nonlinear phenomena, including various types of bifurcation [3–9], mode coupling [10–12], stochastic resonance [13,14], and parametric amplification and oscillations [15–17]. From the perspective of applications, their capabilities of ultrasensitive sensing, such as single-molecule detection [18] and force and mass detection [19–24], have been addressed, and interesting concepts of electronic devices using nanomechanical motion have also been discussed [5,25,26]. Notably, in recent years, there has been considerable interest in nanomechanical computing [27,28]. Nanomechanical memory is realized by exploiting nonlinear behavior with bifurcation dynamics [29]; the vibrational state, which describes the stored information, is switched by the phase-modulated driving force. In Ref. [30], such switching was achieved by application of a dc voltage to the force. Another implementation of the memory uses a buckled nanobeam characterized by a double-well potential [31]. Logic gates for various operations, such as AND, OR, and XOR operations, have also been realized with use of the nonlinear mode in nanomechanical vibrations [32–38]. These features could contribute to promising future nanoscale applications [39,40].

A resonantly driven nanomechanical system can display the bistability of forced vibrations. The range where two stable vibrational states coexist is limited by the bifurcation curves in the plane of the driving amplitude and frequency [5,6]. At the cusp point on these curves, the coexisting states merge. Near this point, a small change in the driving field can lead to switching between the states. This highly sensitive feature is advantageous for sensing applications and quantum measurement [41–43]. In our previous work, we showed that such highly sensitive resonant-mode behavior could be used in signal processing, particularly for the detection of a digitally modulated signal [5]. Exploiting this mode behavior, the resonator can detect quite a weak signal [5,6]. As such a signal is often buried in noise, we investigated the effect of noise in the detection; we revealed that optimization with respect to noise is possible for robust detection.

Here we theoretically address the logic gate with a highly sensitive resonant mode in a nonlinear nanomechanical system. Figure 1(a) shows the system diagram of the logic gate introduced in this work; the resonator works as a bidirectional bifurcation amplifier, whose response is provided in Fig. 1(b) [5]. According to the type of logical computation considered, sequenced data with N bits, $X = [X_1, \ldots, X_j, \ldots, X_N]$, where $X_j \in \{0, 1\}$ and $1 \leq j \leq N$, are encoded in the amplitude of the driving force, $F(t)$. The amplitude is composed of two components, one of which excites the highly sensitive nonlinear mode, and the other of which is the signal, enabling the logical computation for the data X. In the highly sensitive regime, such computation is possible even when the signal is weak. The nanomechanical nonlinear vibration driven by such an encoded driving force performs a logical computation, and the result of the computation $Y \in \{0, 1\}$ is obtained as the final vibrational state.

———————
[*]y.tadokoro@ieee.org
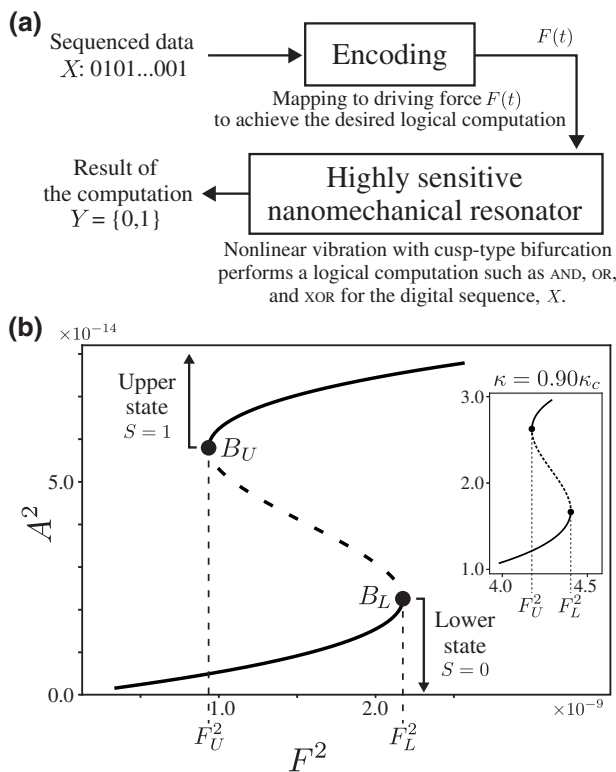
(a)

(b)

FIG. 1. (a) System diagram of a logic gate with a single nanomechanical resonator. According to the desired computation, the input sequence X is encoded in the amplitude of the driving force $F(t)$; see Eq. (3). Exploiting the nonlinear behavior as shown in (b), we obtain the result Y as the final vibrational state. (b) Numerical example of nonlinear response with cusp-type bifurcation ($\kappa \approx 0.28$) [5,6]. When a system is driven close to resonance, the vibrations display bistability: for the same value of the driving-force amplitude F^2, the vibrational squared amplitude A^2 can assume one of the two values of the lower state $S = 0$ or upper state $S = 1$. The inset shows the response in a highly sensitive regime. When the system operates near the critical point, for example, $\kappa = 0.90\kappa_c \approx 0.52$, the resonating vibration is quite sensitive to the driving force; even with a small variation in the driving-force amplitude, it leads to switching to a different vibrational state.

To realize the logic gates for the sequenced data, one critical issue is the required number of resonators; although leading studies have demonstrated the exciting concept of performing a logical operation with resonators, logic gates for such data require many resonators [28,35,44]. To perform a two-bit XOR operation, one resnator is required [32]. This means that the logic gates for an N-bit digital sequence, which often appears in various digital applications, require $N-1$ resonators [35,44]. It has been shown that a single resonator with multiple pumping signals can perform operations with three digital bits [34]. However, many pumping signals are required to achieve this operation, as is a complicated pumping-frequency design. With the delay-based approach of reservoir computing, the

implementation of logic gates using Duffing nonlinearity in a silicon beam was reported by Dion *et al.* [37]. Yao and Hikihara [38] showed that controlling the logical input signal with a feedback loop can realize logical operation in a comb-drive MEMS resonator. Compared with these pioneering studies, the advantageous feature in the method introduced here is that a simple encoding method applied on the driving force can perform a logical operation for sequenced data. Owing to the use of the highly sensitive resonant mode, this method can work even with a weak signal.

II. BRIEF DESCRIPTION OF NONLINEAR RESPONSE IN NANOMECHANICAL SYSTEMS

We briefly describe the vibrational bifurcation dynamics used in our system in this section. Vibrations in a nonlinear mode are often discussed with use of a standard model of vibrational dynamics, the resonantly driven Duffing oscillator [1,2],

$$\ddot{q} + 2\Gamma\dot{q} + \omega_0^2 q + \gamma q^3 = F(t), \qquad (1)$$

where Γ is the friction coefficient, ω_0 is the resonant angular frequency, and γ is the nonlinearity (Duffing) parameter. In nanomechanical systems, the vibrational coordinate q describes, for example, the displacement of the tip of a nanocantilever [18] or of the antinode of a double-clamped nanobeam [19,32,33]. The system is often driven by a periodic force, $F(t) = F \cos \omega_s t$, with force amplitude F and angular frequency ω_s. In cusp-type bifurcation, nonlinear behavior can be observed in the "frequency-detuning" condition, where the driving frequency is close to resonance; that is, $\Delta\omega \equiv |\omega_s - \omega_0| \ll \omega_0$ takes a nonzero value. In the absence of noise, the solution of Eq. (1) is given as $q(t) = A \cos \omega t$, with vibrational amplitude A and motion frequency ω. Classical mechanical theory [45] shows that the frequency ω depends on the amplitude such as $\omega = \omega_0 + (3\gamma/8\omega_0)A^2$, and the squared amplitude A^2 satisfies a nonlinear equation:

$$A^2 \left[\left(\Delta\omega - \frac{3\gamma}{8\omega_0}A^2 \right)^2 + \Gamma^2 \right] = \frac{F^2}{4\omega_0^2}. \qquad (2)$$

Nonlinear behavior is found in the response of the squared amplitude to the driving force. To aid understanding, we provide a numerical example in Fig. 1(b). Here, rewriting $\omega_0 = 2\pi f_0$ and $\omega_s = 2\pi f_s$, we use $f_0 = 1.0$ kHz, $f_s = 1.000\,005\,7$ kHz, $\gamma = 1.0 \times 10^{16}$ m^{-2} s^{-2}, and $\Gamma = 0.01$ s^{-1} to calculate the solution of the nonlinear equation, Eq. (2). In this case, the dimensionless decay rate, which is denoted by $\kappa \equiv \Gamma/\Delta\omega$, is calculated as approximately 0.28. These values strongly depend on the structure of the resonator; practical values can be obtained by measurements and/or theoretical modeling [46,47]. In addition,

such vibration is often observed with physical quantities, such as in an electronic current [19,33,46] or optics [36]. When a system is driven close to resonance, the vibrations display bistability: for the same value of the driving-force amplitude, the vibration amplitude can take on one of two values in either the lower state or the upper state. A binary symbol S indicates in which state the resonator operates: in the lower state $S = 0$, and in the upper state $S = 1$.

A highly sensitive nanomechanical resonator is found in the case when the difference between the bifurcational values of the amplitude of the driving force (i.e., $F_L^2 - F_U^2$) is very small [5]. We can observe such sensitivity when the system operates near the critical point, $\kappa = 1/\sqrt{3} \equiv \kappa_c$. One example of the response with $f_s = 1.000\,003\,1$ kHz, giving $\kappa = 0.90\kappa_c$, is provided in the inset in Fig. 1(b). Even with the small variation in the driving-force amplitude, the system changes to a different state, indicating that the resonating vibration is quite sensitive to variation in the driving force.

III. DESIGN OF DRIVING FORCE IN LOGIC GATES FOR SEQUENCED DATA

The response curve in Fig. 1(b) shows an important characteristic for the development of the logic gate: the resonator physically behaves as a two-state system, and the vibrational state depends on the previous one. When the driving force lies between the bifurcation amplitudes, F_U^2 and F_L^2, the system is kept in the same state regardless of the force amplitude. This "memory effect" is useful in the development of the logic gate because we can save the information corresponding to a critical vibrational state, which determines the result, Y. To reflect the critical state in the result, we originally design the sequential driving force $F(t)$,

$$F(t) = \sum_{j=1}^{N} F_X[j] g_{D_s}\big[t - (j-1)D_s\big] \cos \omega_s t, \qquad (3)$$

where $F_X[j] = F_B + F_s[j]$ is the force amplitude for the data bit X_j. The biased force amplitude F_B satisfying $F_L < F_B < F_U$ excites the resonator. The encoded signal amplitude $F_s[j]$ enables the logical computation with the data bit, X_j. By our denoting $g_\tau(t)$ as a pulsed signal such that $g_\tau(t) = 1$ when $0 \le t < \tau$ and $g_\tau(t) = 0$ otherwise, each data bit is described by a pulsed signal with time duration $D_s \gg 1/\omega_s$. Driving the resonator with this force, we can obtain the result of the computation as the final vibrational state after the driving, namely, $Y = S_N$, where $S_j \equiv S|_{t=jD_s}$. This is achieved by our original encoding method: mapping the input sequenced data X_j to the force amplitude $F_X[j]$. This encoding method depends on the type of logical operation focused on. Here we focus on the three major operations, OR, AND, and XOR operations. In addition to

the proposed concept, other operations can, of course, be considered, including NAND, ONR, and XNOR operations.

A. OR operation

First, we introduce the encoding method for the OR operation, $Y_\vee = X_1 \vee \cdots \vee X_N \equiv \vee_{j=1}^{N} X_j$, where the operator $\vee$ indicates performing the disjunction operation. We design this method on the basis of observation of the OR operation for sequenced data. A truth-value table for OR is provided in Fig. 2(a); we can see that if at least one of the two variables, X_1 and X_2, is equal to 1, the result is $X_1 \vee X_2 = 1$. If this is not the case (i.e., if both variables are equal to 0), we obtain $X_1 \vee X_2 = 0$. These observations indicate that performing the OR operation for the sequence X is described by two cases, case 0 and case 1. The result

(a)

Truth -value table of OR

X_1	X_2	$X_1 \vee X_2$
0	0	0
0	1	1
1	0	1
1	1	1

Case 0
If $X_j = 0$ for all j,
$Y_\vee = \vee_{j=1}^{N} X_j = 0$

Case 1
If $X_j = 1$ exists in $1 \le j \le N$,
$Y_\vee = \vee_{j=1}^{N} X_j = 1$

(b)

Case 1
Do not to change the large vibration when $X_j = 0$ | Excite large vibration when $X_j = 1$ exists
$S = 1$
B_U
Critical vibrational state
$F_U < F_X[j] < F_L$ for $X_j = 0$
$F_X[j] > F_L$ for $X_j = 1$
A^2
B_L
$S = 0$
Keep the small vibration when $X_j = 0$ for all j
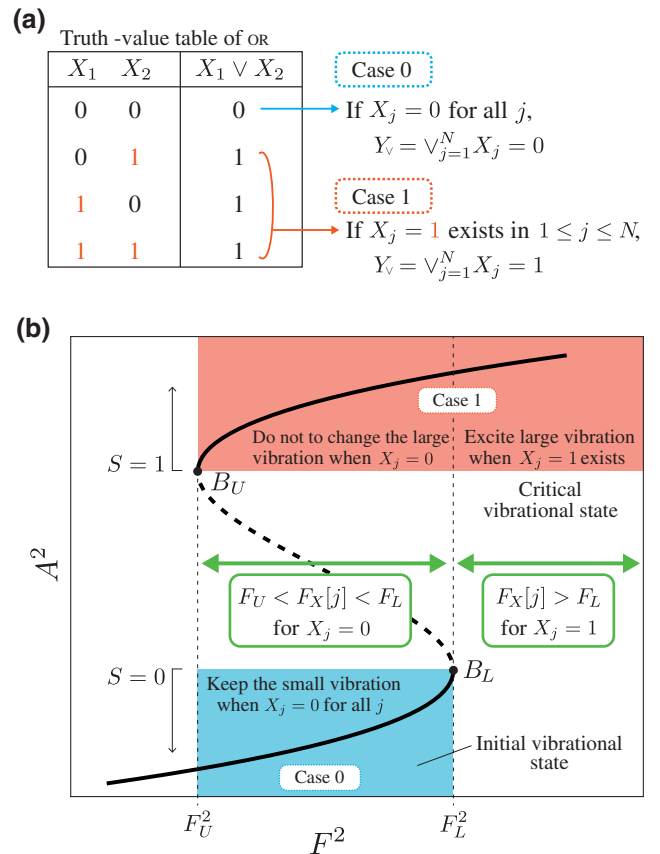Initial vibrational state
Case 0
F_U^2
F^2
F_L^2

FIG. 2. Design of the driving-force amplitude $F_X[j]$ based on the truth-value table for the OR operation. The truth-value table (a) indicates that if $X_j = 0$ for all j, taking the OR operation for X gives the value $Y_\vee = 0$ (case 0). In contrast, if $X_j = 1$ exists in $1 \le j \le N$, we obtain the result $Y_\vee = 1$ (case 1). To enable this calculation with a single nanomechanical resonator, we design the driving force as described in (b); see the green arrows. Case 1 includes the critical vibrational state, because the existence of $X_j = 1$ determines the result $Y_\vee = 1$. To achieve the above behavior, the encoded signal amplitude $F_s[j]$ is designed by Eq. (4).

$Y_\vee$ in case 0 (i.e., if $X_j = 0$ for all j) is $Y_\vee = 0$. In contrast, in case 1, if $X_j = 1$ exists in $1 \leq j \leq N$, we obtain the result $Y_\vee = 1$. This critical value, which determines the result, is represented by the critical vibrational state.

To realize the logical operation in the above two cases, we design the force amplitude, as shown in Fig. 2(b). In case 1, to obtain the result $Y_\vee = 1$, the final vibrational state is the upper one, $S_N = 1$. To achieve this, the resonator should work in the critical vibrational state for $X_j = 1$. We realize this using the force amplitude $F_X[j] > F_L$ for $X_j = 1$, causing the resonator to work beyond the bifurcation point B_L. Even in the opposite case of $X_j = 0$, the vibrational state should be maintained in the upper state to obtain the result $S_N = 1$. This is achieved with the setting $F_U < F_X[j] < F_L$ for $X_j = 0$. Therefore, the force amplitude is designed to stay in the red highlighted region in Fig. 2(b).

In case 0, all data bits included in sequence X take the same value of 0. As the force amplitude $F_X[j]$ corresponding to such a constant sequence takes the same value for all j, the resulting vibrational state is also the same across the whole sequence. To obtain the result $Y_\vee = 0$ (i.e., for the final state to be the lower one, $S_N = 0$), the resonator should continuously work in the lower state (i.e., $S_j = 0$ for all j). Therefore, the force amplitude for this case should be set to meet the condition $F_X[j] < F_L$, and the initial vibrational state should be set as $S_0 = 0$. Combined with case 1, $F_U < F_X[j] < F_L$ for $X_j = 0$ [cyan highlighted region in Fig. 2(b)]. Considering the relation $F_X[j] = F_B + F_s[j]$, the encoded signal amplitude to realize the OR operation for sequence data is

$$F_s[j] = \begin{cases} \delta_\vee & (X_j = 1), \\ 0 & (X_j = 0), \end{cases} \tag{4}$$

where $\delta_\vee > F_L - F_B$ for a given biased force amplitude F_B. When $X_j = 1$, the driving-force amplitude $F_X[j] = F_B + \delta_\vee$ excites the vibration such that $S_j = 1$. The initial value of the amplitude is designed to realize the initial state, $S_0 = 0$. The system becomes highly sensitive when the difference between F_U and F_L is small, as shown in the inset in Fig. 1(b). In this case, even when $\delta_\vee$ is small, the system correctly switches to the other vibrational state. As such a signal is often buried in noise, we investigated the effect of noise in the highly sensitive regime [5]; an optimization with respect to noise is possible for robust logical operations.

B. AND operation

Next we introduce the encoding method for the AND operation, $Y_\wedge = X_1 \wedge \cdots \wedge X_N \equiv \wedge_{j=1}^{N} X_j$, where the symbol $\wedge$ indicates performing the conjunction operation. As in the OR operation, the method is designed on the basis of our observations of the AND operation. A truth-value table for AND is provided in Fig. 3(a); we can see that if at least

(a)

Truth-value table of AND

X_1	X_2	$X_1 \wedge X_2$
0	0	0
0	1	0
1	0	0
1	1	1

Case 0
If $X_j = 0$ exists in $1 \leq j \leq N$,
$Y_\wedge = \wedge_{j=1}^{N} X_j = 0$

Case 1
If $X_j = 1$ for all j,
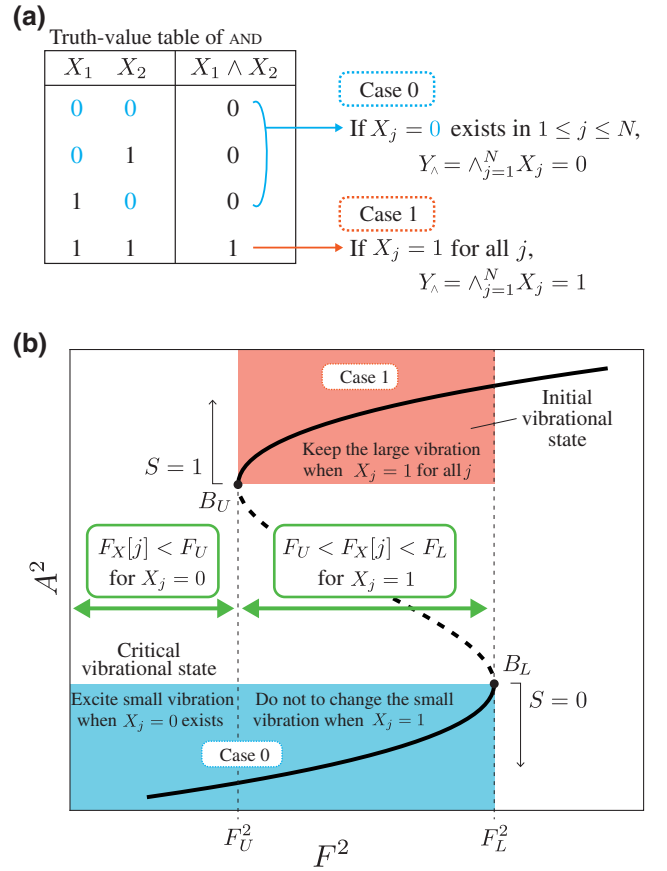$Y_\wedge = \wedge_{j=1}^{N} X_j = 1$

(b)

FIG. 3. Design of the driving-force amplitude $F_X[j]$ based on the truth-value table for the AND operation. According to the truth-value table (a), the driving force, which enables us to perform the AND operation, is set as described in (b). In case 0, the critical vibrational state is found because the existence of $X_j = 0$ determines the result, $Y_\wedge = 0$.

one of the two variables, X_1 and X_2, is equal to 0, the result is $X_1 \wedge X_2 = 0$. If this is not the case, (i.e., if both variables are equal to 1), we obtain $X_1 \wedge X_2 = 1$. These observations indicate that performing the AND operation for sequence X is described by two cases, case 0 and case 1. In case 0 (i.e., if $X_j = 0$ exists in $1 \leq j \leq N$), we obtain the result $Y_\wedge = 0$. In case 1, if $X_j = 1$ for all j, the result is $Y_\wedge = 1$.

On the basis of the above observation, we design the force amplitude for the AND operation, as shown in Fig. 3(b). In case 0, the result is $Y_\wedge = 0$, and the corresponding final vibrational state is the lower one, $S_N = 0$. This result can be obtained with the force amplitude, which belongs to the cyan highlighted region in Fig. 3(b). The critical state for the data bit $X_j = 0$ is realized by $F_X[j] = F_B - \delta_\wedge < F_U$. This indicates that when $X_j = 0$, the encoded signal amplitude is given as $F_s[j] = -\delta_\wedge$ satisfying $\delta_\wedge > F_B - F_U$.

For the opposite case of $X_j = 1$, the vibrational state should be maintained in the lower state. This is achieved with the setting $F_U < F_X[j] < F_L$ for $X_j = 1$. In case 1,

all data bits included in the sequence take the same value of 1. Similarly to case 1 in the OR operation, to obtain the result $Y_\wedge = 1$, the resonator should continuously work in the upper state (i.e., $S_j = 1$ for all j). The force amplitude is designed to meet the condition $F_X[j] = F_B > F_U$ (i.e., $F_s[j] = 0$ when $X_j = 1$), and the initial vibrational state should be set as $S_0 = 1$. Combined with case 0, $F_U < F_X[j] < F_L$ for $X_j = 1$ [red highlighted region in Fig. 3(b)]. The initial value of the amplitude is designed to realize the initial state, $S_0 = 1$.

C. XOR operation

Performing the XOR operation $Y_\oplus = X_1 \oplus \cdots \oplus X_N$ with a nonlinear nanomechanical resonator is achieved by introducing the following "flipping" mapping of the force amplitude:

$$F_X[j] = \begin{cases} -F_X[j-1] & (X_j = 1), \\ F_X[j-1] & (X_j = 0); \end{cases} \quad (5)$$

that is, although the absolute value of the amplitude is equal to the previous one, its sign is flipped depending on the data bit X_j. Here the operator $\oplus$ indicates performing the exclusive disjunction operation. The absolute value is determined such that the system operates outside the bifurcation region; that is, $|F_X[j]| = |F_B + \delta_\oplus|$ satisfying $\delta_\oplus > \max[F_L - F_B, F_B - F_U]$ for a given F_B. With these amplitudes, the resonator works outside the bistable region; the "memory effect" does not exist, and the vibrational state is simply determined as $S_j = -S_{j-1}$ for $X_j = 1$ and as $S_j = S_{j-1}$ for $X_j = 0$, or equivalently, $S_j = S_{j-1} \oplus X_j$. Using the property that $a = b \oplus c \Leftrightarrow c = a \oplus b$ for Boolean variables a, b, and c, we obtain an important relation between the successive states: $X_j = S_j \oplus S_{j-1}$.

When the mapping rule (5) is used, we can analytically show that the final vibrational state S_N is the result of the XOR operation (i.e., $Y_\oplus = S_N$). With the two properties $a \oplus a = 0$ and $a \oplus 0 = a$, in addition to the relation obtained above, the result is

$$\begin{aligned} Y_\oplus &= X_1 \oplus \ldots \oplus X_N \\ &= (S_0 \oplus \underbrace{S_1) \oplus (S_1}_{=0} \oplus \underbrace{S_2) \oplus}_{=0} \cdots \underbrace{\oplus (S_{N-1}}_{=0} \oplus S_N) \\ &= S_0 \oplus S_N. \end{aligned} \quad (6)$$

When the initial vibrational state is set to the lower state (i.e., $S_0 = 0$), we obtain the result, $Y_\oplus = S_N$.

IV. NUMERICAL RESULT OF LOGICAL CALCULATION

We numerically demonstrate our logical calculation method by simulating a single nonlinear nanomechanical resonator. To clearly focus on the behavior of the

vibrational amplitude, we use a method of averaging [5] to eliminate a fast-oscillating mode in the vibration. if we change to dimensionless time $t' \equiv \Delta\omega \cdot t$ and introduce a change of variables, $q = C_{\text{res}}(Q\cos\omega_s t + P\sin\omega_s t)$ and $\dot{q} = -\omega_s C_{\text{res}}(Q\sin\omega_s t - P\cos\omega_s t)$ with $C_{\text{res}} = (8\omega_s\Delta\omega/3\gamma)^{1/2}$, Eq. (1) is represented with two slow variables, Q and P, as $dQ/dt' = -\kappa Q + \partial g/\partial P$ and $dP/dt' = -\kappa P - \partial g/\partial Q$, where the Hamiltonian $g(Q,P) \equiv (Q^2 + P^2 - 1)^2/4 - \beta^{1/2}Q$ and scaled driving force $\beta \equiv 3\gamma F^2/32\omega_s^3(\Delta\omega)^3$. Using the above expressions, we obtain an expression for the vibrational amplitude of $A^2 = C_{\text{res}}^2(P^2 + Q^2)$ without fast-oscillating terms. We numerically calculate P and Q with the settings used in Fig. 1(b) ($\kappa = 0.28$).

The numerical results for the OR operation are provided in Figs. 4(a) and 4(b). Here $F_B = F_M + \varepsilon$ and $\delta_\vee = F_L - F_M$, where $F_M^2 \equiv (F_L^2 + F_U^2)/2$ is the mean of the squared bifurcation amplitudes, and small constant $\varepsilon = 6.2 \times 10^{-9}$. In Fig. 4(a), for the input sequence $X = [0, 1, 0, 0, 0, 1, 0]$, the initial vibrational state is set to the lower state, $S_0 = 0$, and Eq. (4) gives us the driving force β that achieves the calculation. The resulting final vibrational state is $S_7 = 1$, which equals the answer $Y_\vee = 1$. Notably, even with the long sequences, $N = 7$ in Fig. 4(a) and $N = 4$ in Fig. 4(b), the single resonator can correctly compute the logical value. Another example is found in Fig. 4(b); for $X = [0, 0, 0, 0]$, the final vibrational state is $S_4 = 0$, and we obtain the correct result $Y_\vee = 0$. For the AND operation, Figs. 4(c) and 4(d) show the results with the settings $F_B = F_M + \varepsilon$ and $\delta_\wedge = F_M - F_U - 2\varepsilon$. With the initial vibrational state of $S_0 = 1$ and the designed sequential driving force, we obtain the correct results of the calculation for two input sequences.

For the remaining logical operation of our focus, XOR, Figs. 4(e) and 4(f) show the numerical results with the settings $F_B = F_M$ and $\delta_\oplus = F_L - F_M + \varepsilon$. The initial state is set to the lower state, $S_0 = 0$. In the XOR operation, the number of the data bit $X_j = 1$ is counted, and the obtained number in modulo 2 is the result. Owing to the introduced "flipping" mapping, this data bit induces a change of state, and the result is found in the final vibrational state. Indeed, in Fig. 4(e), the number of $X_j = 1$ is 3, which corresponds to the change of the state. The final state $S_5 = 1$ gives the result: $Y_\oplus = 1$. Another example in Fig. 4(f) also gives the correct result, $Y_\oplus = 0$.

Figure 5 shows the result of the OR calculation when the system operates near the critical point, $\kappa = 0.90\kappa_c$. Here $F_B = F_M$ and $\delta_\vee = F_L - F_M + \varepsilon$ with the small constant $\varepsilon = 1.9 \times 10^{-12}$. Compared with Fig. 4(a), this setting realizes a weak encoded signal amplitude; see Fig. 5(a). Even with this small variation, Fig. 5 shows that the proposed method with the nonlinear nanomechanical resonator successfully executes the OR operation. The operation close to the cusp point is vulnerable and must be performed with care in the presence of noise. As discussed
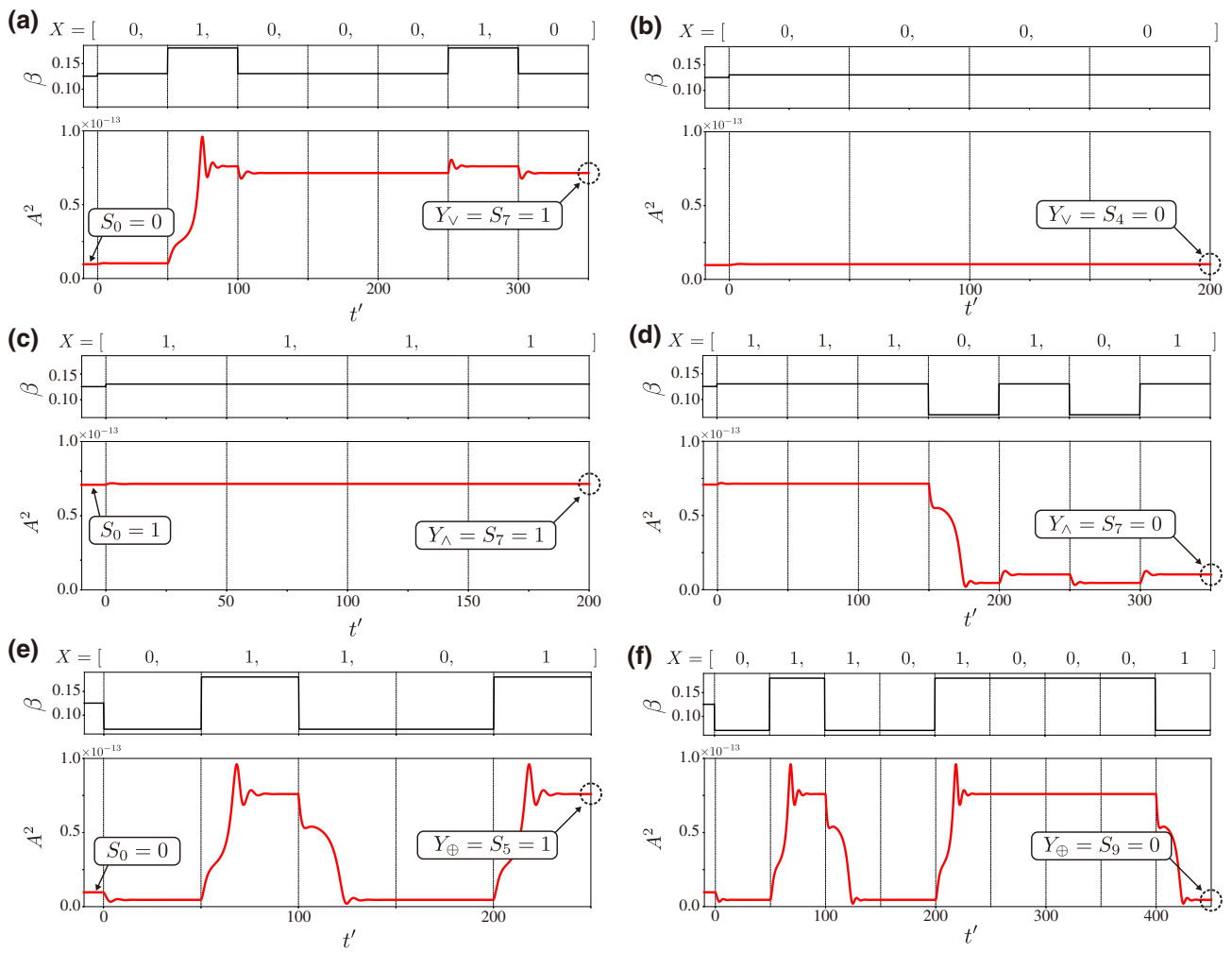
FIG. 4. Numerical results of logical computation for the sequenced data X for (a),(b) the OR operation, (c),(d) the AND operation, and (e),(f) the XOR operation. In each figure, we use different sequenced data to aid understanding of the universality of the proposed method. Owing to the adequate setting of the initial vibrational state and our designed force β, all results are correctly obtained as the final vibrational state.

in Refs. [5,48], noise can cause unexpected switching between the states, which leads to an error. The probability that erroneous switching is observed increases exponentially with decreasing encoded signal amplitude, $\delta_\vee$. In the logical-computation framework introduced, we must consider the case where such an amplitude is sufficiently larger than the noise level.

One of the essential factors in logical computation is calculation speed. In the system introduced , this speed is determined mainly by damping. In the equation of motion (1) taken as the focus of this work, the damping is described by the term Γ. The damping factor determines the time duration in which the vibration reaches a stable state. To correctly obtain the solution of the logical operation, we must wait until the vibration is stabilized every time the driving-force amplitude changes. This means that the calculation speed depends on the damping.

Increasing Γ leads to a decrease in the time duration, meaning increase of the calculation speed.

V. CONCLUDING REMARKS

We theoretically introduce a simple method to achieve logic gates for sequenced data. A nanomechanical resonator is operated as a bidirectional bifurcation amplifier and, according to the input digital sequence, the amplitude of the driving force is encoded to achieve the desired logical operation. Focusing on the highly sensitive regime, we demonstrated that such operations can be performed even with a small variation in the amplitude of the driving force or signal. The numerical results showed that a single resonator successfully works as a logic gate for the three major logical operations, AND, OR, and XOR, even for long digital sequences. The principles that underlie
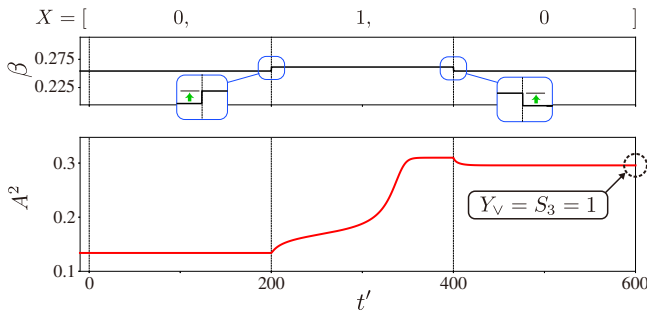
FIG. 5.   OR calculation when the system operates near the critical point ($\kappa = 0.90\kappa_c$). Although the encoded signal amplitude is quite small (see the green arrows), the proposed method with the nonlinear nanomechanical resonator successfully executes the OR operation.

bifurcation topology are simple and generic, suggesting that our method is applicable not only to nanomechanical systems but also to a wide variety of physical, chemical, and biological systems with bifurcation dynamics.

The system introduced is quite sensitive to thermal noise in the highly sensitive regime. As κ approaches κ_c, namely, $|F_U^2 - F_L^2|$ goes to zero, the system may often be switched to a different state by noise at random. Our theoretical analysis in Ref. [5], as well as previous theoretical work and experimental work on nanomechanical systems [49,50], shows that the probability of such erroneous switching is determined by the relation between the distance to the critical point in the parameter space and the noise intensity. It exponentially increases with the increase of the noise intensity. However, noise in nanomechanical systems is usually small, and with very few exceptions the experiments on noise-induced interstate switching in nanomechanical and micromechanical systems were done by adding external noise rather than relying on the intrinsic noise of the device. As we showed in Ref. [5], for realistic weak noise, one can have a very reliable switching in response to a weak signal in the highly sensitive regime while still being very weakly affected by the noise.

Our method has been designed for a single type of logic operation such as $X_1 \vee X_2 \vee X_3 \vee X_4$, leading to universality for this type of logic operation. When a different type of logic is included [e.g., $(X_1 \wedge X_2) \vee (X_3 \wedge X_4)$], use of a memory device enables our method to perform the logical operation. Such a memory device is required to store the temporal result of the prioritized calculations, such as $(X_1 \wedge X_2)$ and $(X_3 \wedge X_4)$ in the above example. The remaining "$\vee$" operation is performed on the basis of the stored results. Even when a different type of logic is considered, our method without memory is still effective for a particular type of logic; that is, nested logic: $((X_1 \wedge X_2) \vee X_3) \wedge X_4$. In this case, along with the prioritized operation order, our method can be performed with the introduced encoded driving force.

[1] S. Schmid, L. G. Villanueva, and M. L. Roukes, *Fundamentals of Nanomechanical Resonators* (Springer, Cham, 2016).

[2] M. I. Dykman, *Fluctuating Nonlinear Oscillators: From Nanomechanics to Quantum Superconducting Circuits* (University Press, Oxford, 2012).

[3] D. A. Czaplewski, S. Strachan, O. Shoshani, S. W. Shaw, and D. López, Bifurcation diagram and dynamic response of a mems resonator with a 1:3 internal resonance, Appl. Phys. Lett. **114**, 254104 (2019).

[4] S. Houri, D. Hatanaka, M. Asano, R. Ohta, and H. Yamaguchi, Limit cycles and bifurcations in a nonlinear mems resonator with a 1:3 internal resonance, Appl. Phys. Lett. **114**, 103103 (2019).

[5] Y. Tadokoro, H. Tanaka, and M. I. Dykman, Driven nonlinear nanomechanical resonators as digital signal detectors, Sci. Rep. **8**, 11284 (2018).

[6] M. Defoort, V. Puller, O. Bourgeois, F. Pistolesi, and E. Collin, Scaling laws for the bifurcation escape rate in a nanomechanical resonator, Phys. Rev. E **92**, 050903 (2015).

[7] R. J. Dolleman, P. Belardinelli, S. Houri, H. S. J. van der Zant, F. Alijani, and P. G. Steeneken, High-frequency stochastic switching of graphene resonators near room temperature, Nano Lett. **19**, 1282 (2019).

[8] P. Zhou, X. Dong, C. Stambaugh, and H. B. Chan, Work fluctuations in a nonlinear micromechanical oscillator driven far from thermal equilibrium, Phys. Rev. E **91**, 052110 (2015).

[9] S. Houri, D. Hatanaka, M. Asano, and H. Yamaguchi, Demonstration of Multiple Internal Resonances in a Microelectromechanical Self-Sustained Oscillator, Phys. Rev. Appl. **13**, 014049 (2020).

[10] H. J. R. Westra, M. Poot, H. S. J. van der Zant, and W. J. Venstra, Nonlinear Modal Interactions in Clamped-Clamped Mechanical Resonators, Phys. Rev. Lett. **105**, 117205 (2010).

[11] A. Z. Hajjaj, M. A. Hafiz, and M. I. Younis, Mode coupling and nonlinear resonances of mems arch resonators for bandpass filters, Sci. Rep. **7**, 41820 (2017).

[12] S. Cho, S. U. Cho, M. Jo, J. Suh, H. C. Park, S. G. Kim, S.-B. Shim, and Y. D. Park, Strong Two-Mode Parametric Interaction and Amplification in a Nanomechanical Resonator, Phys. Rev. Appl. **9**, 064023 (2018).

[13] R. L. Badzey and P. Mohanty, Coherent signal amplification in bistable nanomechanical oscillators by stochastic resonance, Nature **437**, 995 (2005).

[14] A. Chowdhury, S. Barbay, M. G. Clerc, I. Robert-Philip, and R. Braive, Phase Stochastic Resonance in a Forced Nanoelectromechanical Membrane, Phys. Rev. Lett. **119**, 234101 (2017).

[15] A. Leuch, L. Papariello, O. Zilberberg, C. L. Degen, R. Chitra, and A. Eichler, Parametric Symmetry Breaking in a Nonlinear Resonator, Phys. Rev. Lett. **117**, 214101 (2016).

[16] I. Mahboob and H. Yamaguchi, Bit storage and bit flip operations in an electromechanical oscillator, Nat. Nanotechnol. **3,** 275 (2008).

[17] J. M. Miller, D. D. Shin, H.-K. Kwon, S. W. Shaw, and T. W. Kenny, Phase Control of Self-Excited Parametric Resonators, Phys. Rev. Appl. **12,** 044053 (2019).

[18] V. Puller, B. Lounis, and F. Pistolesi, Single Molecule Detection of Nanomechanical Motion, Phys. Rev. Lett. **110,** 125501 (2013).

[19] J. Moser, J. Guttinger, A. Eichler, M. J. Esplandiu, D. E. Liu, M. I. Dykman, and A. Bachtold, Ultrasensitive force detection with a nanotube mechanical resonator, Nat. Nanotechnol. **8,** 493 (2013).

[20] M. S. Hanay, S. I. Kelber, C. D. O'Connell, P. Mulvaney, J. E. Sader, and M. L. Roukes, Inertial imaging with nanomechanical systems, Nat. Nanotechnol. **10,** 339 (2015).

[21] R. S. Decca, D. Lopez, E. Fischbach, and D. E. Krause, Measurement of the Casimir Force between Dissimilar Metals, Phys. Rev. Lett. **91,** 050402 (2003).

[22] S. L. de Bonis, C. Urgell, W. Yang, C. Samanta, A. Noury, J. Vergara-Cruz, Q. Dong, Y. Jin, and A. Bachtold, Ultrasensitive displacement noise measurement of carbon nanotube mechanical resonators, Nano Lett. **18,** 5324 (2018).

[23] K. Y. Fong, M. Poot, and H. X. Tang, Nano-optomechanical resonators in microfluidics, Nano Lett. **15,** 6116 (2015).

[24] I. K. Kim and S. I. Lee, Theoretical investigation of nonlinear resonances in a carbon nanotube cantilever with a tip-mass under electrostatic excitation, J. Appl. Phys. **114,** 104303 (2013).

[25] S. T. Bartsch, A. Rusu, and A. M. Ionescu, Phase-locked loop based on nanoelectromechanical resonant-body field effect transistor, Appl. Phys. Lett. **101,** 153116 (2012).

[26] S. Ilyas, K. N. Chappanda, and M. I. Younis, Exploiting nonlinearities of micro-machined resonators for filtering applications, Appl. Phys. Lett. **110,** 253508 (2017).

[27] H. B. Robert, Q. Hua, K. Hyun-Seok, and M. Robert, A nanomechanical computer–exploring new avenues of computing, New J. Phys. **9,** 241 (2007).

[28] M. A. A. Hafiz, L. Kosuru, and M. I. Younis, Towards electromechanical computation: An alternative approach to realize complex logic circuits, J. Appl. Phys. **120,** 074501 (2016).

[29] D. N. Guerra, M. Imboden, and P. Mohanty, Electrostatically actuated silicon-based nanomechanical switch at room temperature, Appl. Phys. Lett. **93,** 033515 (2008).

[30] H. Noh, S.-B. Shim, M. Jung, Z. G. Khim, and J. Kim, A mechanical memory with a dc modulation of nonlinear resonance, Appl. Phys. Lett. **97,** 033116 (2010).

[31] M. Bagheri, M. Poot, M. Li, W. P. H. Pernice, and H. X. Tang, Dynamic manipulation of nanomechanical resonators in the high-amplitude regime and non-volatile mechanical memory operation, Nat. Nanotechnol. **6,** 726 (2011).

[32] M. A. A. Hafiz, L. Kosuru, and M. I. Younis, Microelectromechanical reprogrammable logic device, Nat. Commun. **7,** 11137 (2016).

[33] D. N. Guerra, A. R. Bulsara, W. L. Ditto, S. Sinha, K. Murali, and P. Mohanty, A noise-assisted reprogrammable nanomechanical logic gate, Nano Lett. **10,** 1168 (2010).

[34] I. Mahboob, E. Flurin, K. Nishiguchi, A. Fujiwara, and H. Yamaguchi, Interconnect-free parallel logic circuits in a single mechanical resonator, Nat. Commun. **2,** 198 (2011).

[35] J.-S. Wenzler, T. Dunn, T. Toffoli, and P. Mohanty, A nanomechanical fredkin gate, Nano Lett. **14,** 89 (2014).

[36] S. C. Masmanidis, R. B. Karabalin, I. De Vlaminck, G. Borghs, M. R. Freeman, and M. L. Roukes, Multifunctional nanomechanical systems via tunably coupled piezoelectric actuation, Science **317,** 780 (2007).

[37] G. Dion, S. Mejaouri, and J. Sylvestre, Reservoir computing with a single delay-coupled non-linear mechanical oscillator, J. Appl. Phys. **124,** 152132 (2018).

[38] A. Yao and T. Hikihara, Logic-memory device of a mechanical resonator, Appl. Phys. Lett. **105,** 123104 (2014).

[39] B. Atakan and O. Akan, Carbon nanotube-based nanoscale ad hoc networks, IEEE Commun. Mag. **48,** 129 (2010).

[40] T. Nobunaga, H. Tanaka, and Y. Tadokoro, Reconstruction for spatially distributed single-pixel imaging based on pattern filtering, IEEE Signal Process. Lett. **25,** 705 (2018).

[41] R. Vijay, M. H. Devoret, and I. Siddiqi, The josephson bifurcation amplifier, Rev. Sci. Instr. **80,** 111101 (2009).

[42] K. W. Murch, E. Ginossar, S. J. Weber, R. Vijay, S. M. Girvin, and I. Siddiqi, Quantum state sensitivity of an autoresonant superconducting circuit, Phys. Rev. B **86,** 220503 (2012).

[43] G. Ithier, G. Tancredi, and P. J. Meeson, Direct spectrum analysis using a threshold detector with application to a superconducting circuit, New J. Phys. **16,** 055010 (2014).

[44] M. A. A. Hafiz, R. Li, M. I. Younis, and H. Fariborzi, A parity checker circuit based on microelectromechanical resonator logic elements, Phys. Lett. A **381,** 843 (2017).

[45] L. D. Landau and E. M. Lifshitz, *Mechanics*, Course of Theoretical Physics (Elsevier, Amsterdam, 1976), 3rd ed.

[46] A. Eichler, J. Moser, J. Chaste, M. Zdrojek, I. Wilson-Rae, and A. Bachtold, Nonlinear damping in mechanical resonators made from carbon nanotubes and graphene, Nat. Nanotechnol. **6,** 339 (2011).

[47] I. Kozinsky, H. W. C. Postma, I. Bargatin, and M. L. Roukes, Tuning nonlinearity, dynamic range, and frequency of nanomechanical resonators, Appl. Phys. Lett. **88,** 253101 (2006).

[48] Y. Tadokoro, H. Tanaka, and M. I. Dykman, Noise-induced switching from a symmetry-protected shallow metastable state, Sci. Rep. **10,** 10413 (2020).

[49] M. I. Dykman and M. A. Krivoglaz, Theory of fluctuational transitions between stable states of a nonlinear oscillator, Zh. Eksp. Teor. Fiz. **77,** 60 (1979).

[50] J. S. Aldridge and A. N. Cleland, Noise-Enabled Precision Measurements of a Duffing Nanomechanical Resonator, Phys. Rev. Lett. **94,** 156403 (2005).